JOURNAL OF MATERIALS SCIENCE 31 (1996) 1741–1750

Particle size control of 1,3,5-triamino-2,4,6-trinitrobenzene by recrystallization from DMSO

M. F. FOLTZ, J. L. MAIENSCHEIN, L. G. GREEN
Lawrence Livermore National Laboratory, P.O. Box 808, L-282 Livermore, CA 94550, USA

Batches of up to 46 g of the insensitive explosive 1,3,5-triamino-2,4,6-trinitrobenzene (TATB) have been recrystallized from DMSO in an effort to prepare larger particle-size material for recycling previously-used TATB and also for use in special formulations. The first part of the study investigated the conditions required to shift the particle-size distribution maximum from ~50–70 μm to several hundred micrometres in diameter. Distributions peaking at ~200–246 μm were successfully produced by varying the cooldown rate and degree of agitation during cooling. The second part of the study emphasized regeneration of the standard ~50–70 μm distribution from submicron size ("ultrafine" TATB) particles. The distributions peaking at ~76–88 μm, ~27–31 μm, and ~15–17 μm, successfully bracketed the target particle sizes, were grown by changing the degree of solution saturation. The choice of saturation temperature for the TATB/DMSO solution was based on earlier small-scale recrystallization and solubility work.

1. Introduction

The particle size distribution of the insensitive high explosive (HE) 1,3,5-triamino-2,4,6-trinitrobenzene (triaminotrinitrobenzene, TATB) [1] as manufactured, typically peaks around 50–70 μm [2]. TATB containing predominantly submicrometre particles ("ultrafine") is also available [3]. It is sometimes desirable, however, to modify the particle size distributions to give larger particles. One such instance is the use of TATB in an extrudable paste HE, where a significant fraction of the particles must be 200 μm or greater to attain a low viscosity paste extrudable explosive (PEX) formulation with high solids loading and energy density [4, 5]. Another case is the recovery of TATB for reuse. The recovered TATB is generally of smaller particle size than the original material, and must be treated to increase the particle size distribution to that of the starting material.

Here we report work on the recrystallization of TATB from solutions of TATB and dimethylsulfoxide (DMSO). Past attempts to crystallize large quantities of TATB with dimensions >200 μm, using other solvents, have met with limited success because of the low solubility of TATB [6] although a high-temperature dry amination process was reported to yield ~100 μm size pitted crystals [7]. We chose DMSO as a solvent because of its relatively high solubility for TATB when compared with most common solvents [6, 8]. We have described the methods used to crystallize TATB from DMSO under thermally controlled conditions in an earlier paper [8]. The first part of this paper ("resized distribution") reports on the study of conditions necessary to shift the particle-size distribution from a peak ~50–70 μm to one around several hundred micrometres. The second part of this paper ("size regeneration") discusses work done to regenerate the ~50–70 μm distribution from ultrafine TATB starting material.

2. Experimental

2.1. Resized distribution

The experimental schematic used for crystallizing the TATB in both studies is shown in Fig. 1. To obtain saturation at the maximum temperature of 125 °C, ~23 g of TATB were added to 6 litres of spectrophotometric grade DMSO in a 12-litre three-necked Pyrex round bottomed flask. Solution concentrations were based on data from the earlier crystallization and solubility study [8]. The flask was heated either solely from below, or from both above and below, with heating mantles. The temperature of both heating mantles was monitored with a multichannel Fluke digital thermometer (model 2166A). The upper half of the round bottom flask was insulated with either the deactivated upper heating mantle or glass wool when the system was heated only from below. The solution temperature was controlled with an Omega programmable temperature controller (series 2010) via a K-type thermocouple probe with a stainless steel sheath inserted into the solution through a rubber septum. This septum was later wrapped in a teflon filter membrane (Zitex) to prevent decomposition of the rubber due to exposure to DMSO vapour. We found that the use of teflon-coated thermocouple probes instead of bare metal probes greatly reduced the rate of TATB thermal decomposition, supposedly radical-initiated [8]. A computer-driven thermal override system was used to prevent accidental overheating of the TATB/DMSO solution. This system consisted of a second K-type thermocouple probe in the solution interfaced with a Hewlett Packard

0022–2461

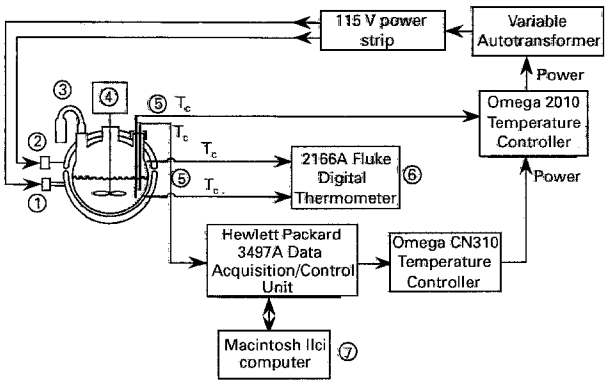

Figure 1 The experimental schematic for growing large-scale batches of crystalline TATB from DMSO. Designations are as follows: (1) and (2) heating mantles; (3) moisture-indicating dessicant ($CaSO_4$); (4) variable speed mixer; (5) four type K thermocouple probes; two having stainless steel sheaths – the two in solution are teflon-coated, one providing feed-back for the Omega 2010 programmable thermal controller, the other providing computerized thermal override protection; (6) monitors top and bottom type K thermocouple probes at the interface between glass and heating mantles (1) and (2); (7) Macintosh computer with software program designed to shut off power to system when a maximum temperature is reached in solution.

(model 3497A) data acquisition/control unit and Macintosh computer, which would turn off the heater power if the control unit malfunctioned and the solution overheated.

The TATB/DMSO solution was heated for an hour and a half at a linear heating rate of $\sim 1.1\,^{\circ}C\,min^{-1}$ from ambient to the programmed maximum temperature of 125 °C. This temperature was chosen as a standard for all runs because it is about the upper limit of the pressurized boiler heating system that would be used in future larger scale-up attempts. The maximum temperature was maintained for at least an hour and a half to provide more time for the solids to dissolve. The solution was visually inspected for remaining undissolved solids before the cooldown cycle was started. On those occasions when undissolved particles were seen, more time (usually about 30 min) was allowed for further dissolution. A glass rod assembly suspended a teflon stirrer blade above the bottom of the flask to avoid grinding crystals that accumulated there during cooldown. The rate of stirring was regulated by a Cole Parmer solid state controller (model 4555-30) with vigorous stirring (~100 rpm) to optimize the degree of solvation during the heat cycle. During the cooldown cycle, the rate of agitation ranged from vigorous to medium (~60 rpm), to slow (~25 rpm), or to no stirring at all. Seed crystals ($\geqslant$200 μm diameter) were added to some batches at the beginning of the cooldown cycle.

Cooling times were on the order of two days, with cooling ramps defined by the rate of change of solubility with time (dS/dt) as either constant (i.e. a constant change in solubility with time) or accelerated (i.e. for each successive 10 °C interval, dS/dt was increased by a factor of two). This method differs from the earlier small-scale crystallization work [2] which used cooling ramps linear with temperature (dT/dt a constant). We found that ramps defined by dS/dt were more time efficient, an important factor in avoiding prolonged high temperatures leading to excessive TATB thermal decomposition, and that they allowed better control of crystal growth. Fig. 2 shows typical cooling (dT/dt) and solubility curves illustrating (a) constant dS/dt and (b) accelerated dS/dt cooldown rates.

Samples for particle-size analysis were obtained by siphoning material off the bottom of the flask with an inverted pipette, or by dragging a scoop across the bottom, both methods providing consistent particle-size results. These 1–2 g samples were filtered through ashless filter paper, and fractionated by weight with manual sieving (USA standard testing sieves, size openings: 1.000, 0.710, 0.500, 0.355, 0.300, 0.246, 0.200 μm) to yield particle-size distributions. A grounded electrostatic wrist guard was used during sieving because static electricity pick-up by fine TATB crystals made the samples otherwise hard to confine during handling. The relatively slow filtering of the entire batch of crystallized TATB was done through a fibrous teflon filter membrane (Zitex, 10–20 μm mean poresize) to reduce contamination of the reused solvent by DMSO dissolved cellulose.

2.2. Size regeneration

The degree of supersaturation on the particle-size distribution was studied by weighing out sufficient ultrafine TATB into 6 litres of DMSO to make just saturated, 1.5× saturated and 2× saturated solutions at 125 °C [8]. For the 1.5× supersaturated solution, for example, enough TATB was weighed out to

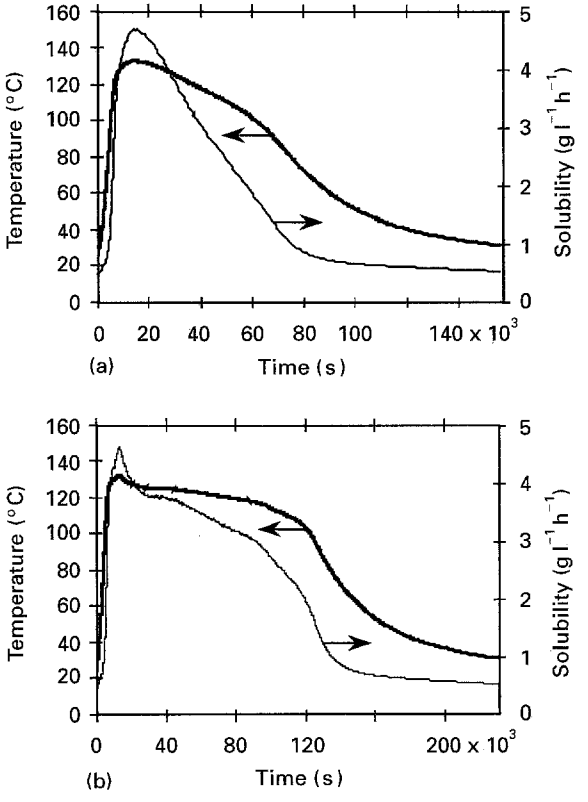

Figure 2 Typical cooling and solubility curves for (a) constant dS/dt, and (b) accelerated dS/dt cooldown rates ("resized distribution" study).

produce a saturated solution at 125 °C with half again as much material left undissolved (i.e. 150% of saturation). Ultrafine TATB was used as starting material for this series of experiments to emulate the very fine particle-size material expected in the recovery of TATB from munitions formulations. The same experimental setup was used as described above, except that the upper part of the flask was insulated with glass wool and thermal control was turned off during the cooldown cycle. The stirring rate was vigorous (~ 100 rpm), except for one run with no stirring during the cooldown period. Typical dT/dt cooling and dS/dt solubility curves are shown in Fig. 3. After each run, the filtered solution was cleaned by mixing it with activated charcoal, which was then separated out by filtration through two layers of Zitex teflon filter membrane. This step was added to the procedure to remove impurities from TATB and DMSO thermal degradation that accumulated in the solution during each run.

Particle-size distributions were determined for this study with a Malvern 3600 laser diffraction particle-size analyzer [9]. Water was used as the carrier medium and wetting agent, and for sonication of the ~ 1 g samples.

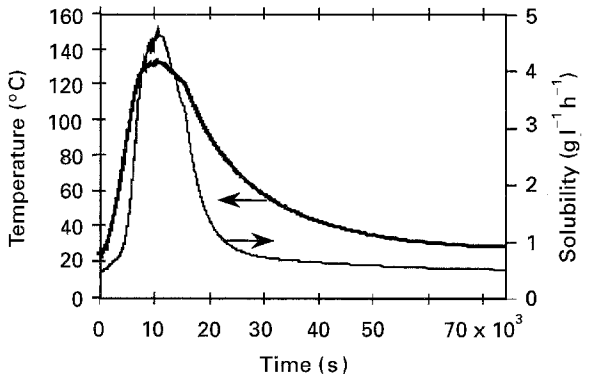

Figure 3 Typical cooling curve obtained when the heating mantle was turned off and the system allowed to cool without programmable control ("size regeneration" study).

3. Results and discussion

3.1. Resized distribution

The particle-size distribution data obtained under various conditions are given in Table I and in Fig. 4(a–j). We also visually noted the morphology of the crystals obtained for each run; representative scanning electron micrographs (SEMs) are shown in Figs 5 and 6.

The two factors that most significantly affected the particle size distribution and crystal shape were the stirring rate and the cooling rate (i.e. constant or accelerated dS/dt). The crystal shape was most strongly affected by stirring rate. Slow and medium stir rates (Fig. 4(a–d)) produced flat hexagonal-shaped crystals of varying thickness, far from the ideal spherical shape desired for formulation purposes [10]. Fast stirring, however, did produce more spherical crystals, as shown in Figs 5 and 6, although they were still somewhat irregular in shape. Fast stirring also produced particle size distributions with relatively larger particles, as shown in Table I and Fig. 4.

We also observed that, with fast stirring, an accelerated dS/dt rate gave a narrower particle size distribution than a constant dS/dt rate. We explain this qualitatively as follows. A fast initial dS/dt will lead to "crashing out", or formation of large numbers of small crystals. This is undesirable, since to get large particles we need relatively few nucleation sites for subsequent crystallization. Therefore, a slow initial dS/dt rate is necessary. However, once the initial particles are formed, we want to quickly crystallize the remaining dissolved material on them before it can nucleate and form more small particles; the crystal growth rate is increased by increasing the dS/dt rate. The use of accelerating dS/dt rates appears to be a key for producing narrow particle size distributions. SEMs of crystals grown with constant and accelerated dS/dt, given in Fig. 5, show little change in crystal morphology between the two cooling methods. In addition to the effect on particle size, the use of accelerated dS/dt is advantageous in reducing the overall duration of recrystallization, and hence reducing the extent of

TABLE I Particle-size data for resized distribution study

Stir rate	Slow	Slow	Slow	Medium	Fast	Fast	Fast	Fast	Fast	Fast
Seeds	No	No	No	No	~1.1 g 200–250 μm	No	~2.0 g 300–500 μm	No	No	No
dS/dt	Constant	Constant	Constant	Constant	Constant	Constant	Constant	Constant	Constant	Accelerated
BHT	No	No	No	No	No	No	No	3.7×10^{-3} M	1.5×10^{-2} M	1.5×10^{-2} M
Number of heating mantles	2	2	2	2	2	1	1	1	1	1
Sieve size (mm)	Weight fraction									
> 1.000	0.0000	0.0000	0.0000	0.0000	0.0000	0.0000	0.0000	0.0004	0.0000	0.0000
0.711–1.000	0.0004	0.0025	0.0003	0.0000	0.0000	0.0000	0.0002	0.0004	0.0000	0.0000
0.501–0.710	0.0188	0.0115	0.0074	0.0107	0.0027	0.0094	0.0140	0.0171	0.0065	0.0002
0.356–0.500	0.0718	0.0455	0.0795	0.0396	0.0375	0.1120	0.0632	0.1495	0.0892	0.0030
0.301–0.355	0.0498	0.0239	0.0654	0.0364	0.0972	0.1691	0.0422	0.1391	0.1364	0.0146
0.247–0.300	0.0617	0.0268	0.0733	0.1120	0.2545	0.2657	0.1372	0.2625	0.2919	0.1242
0.201–0.246	0.7059	0.6416	0.6128	0.6760	0.5648	0.3968	0.6700	0.4174	0.4215	0.8249
< 0.200	0.0917	0.2483	0.1617	0.1253	0.0433	0.0470	0.0734	0.0307	0.0546	0.0332
Fig. 4:	a	b	c	d	e	f	g	h	i	j

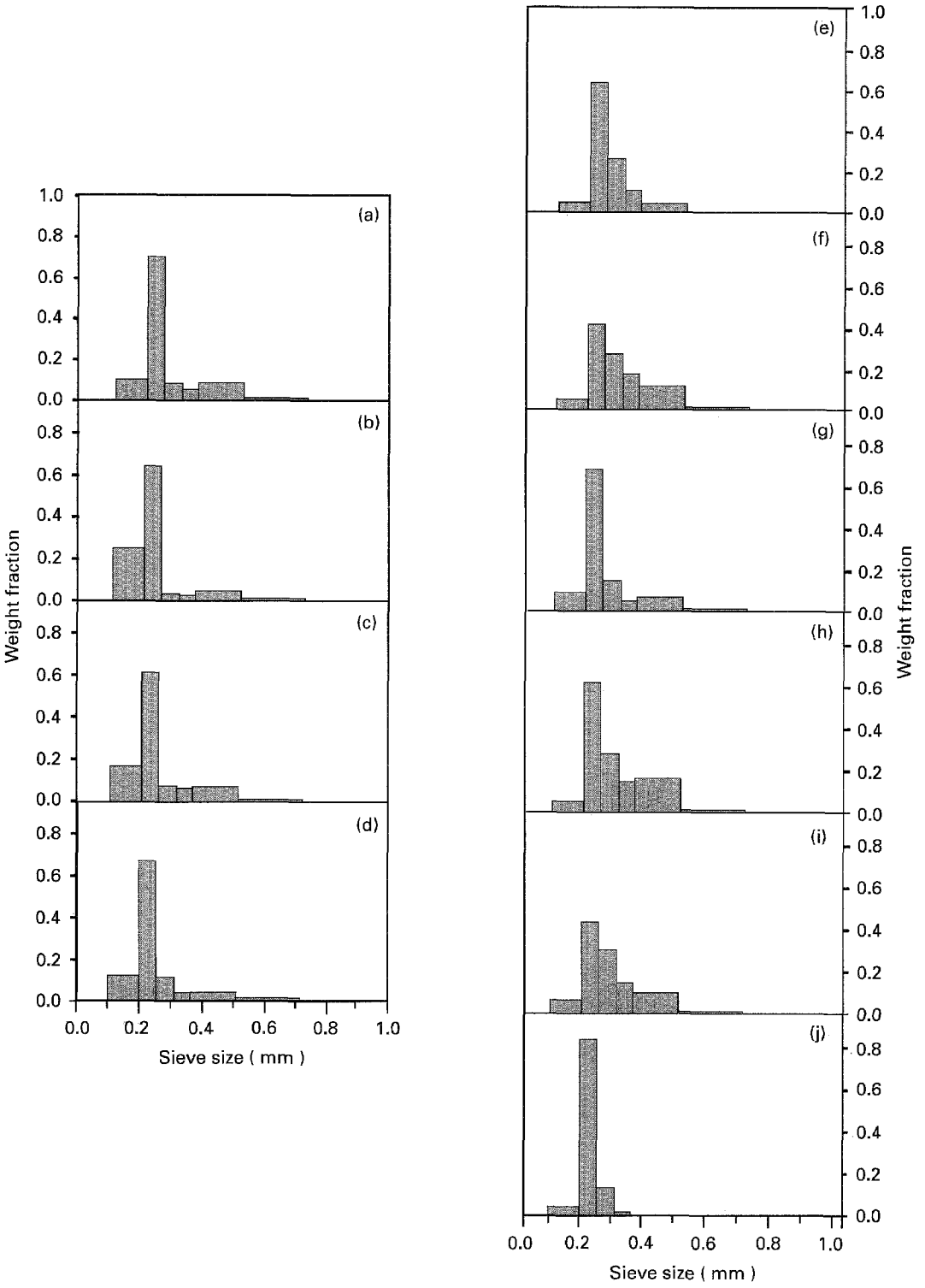

Figure 4 Particle-size distributions determined by manually sieving 1–2 g samples of TATB grown under various conditions (see Table I).

thermal degradation of the TATB and DMSO during recrystallization.

A qualitative insight into the effect of stirring speed on particle size distribution may be drawn from mass transfer considerations. We assume that the rate of crystallization is controlled by the relatively slow diffusional transfer of dissolved TATB through the stagnant boundary layer at the surface of each particle. In this case, the molar flux of TATB to the particle surface is given by [11]

$$\text{Molar flux} = \left(4\pi CD \Big/ \left(\frac{1}{r_1} - \frac{1}{r_2}\right)\right) \times \ln\left(\frac{C_\infty}{C_s}\right) \quad (1)$$

where: molar flux = rate of transfer of TATB to the particle surface, $\text{mol}\,\text{s}^{-1}$, C = total molar concentration of solution, $\text{mol}\,\text{m}^{-3}$, D = diffusion constant for TATB in solution, $\text{m}^2\,\text{s}^{-1}$, r_1 = radius of solid particle, m, r_2 = radius of edge of stagnant boundary layer around particle, m, C_∞ = TATB concentration

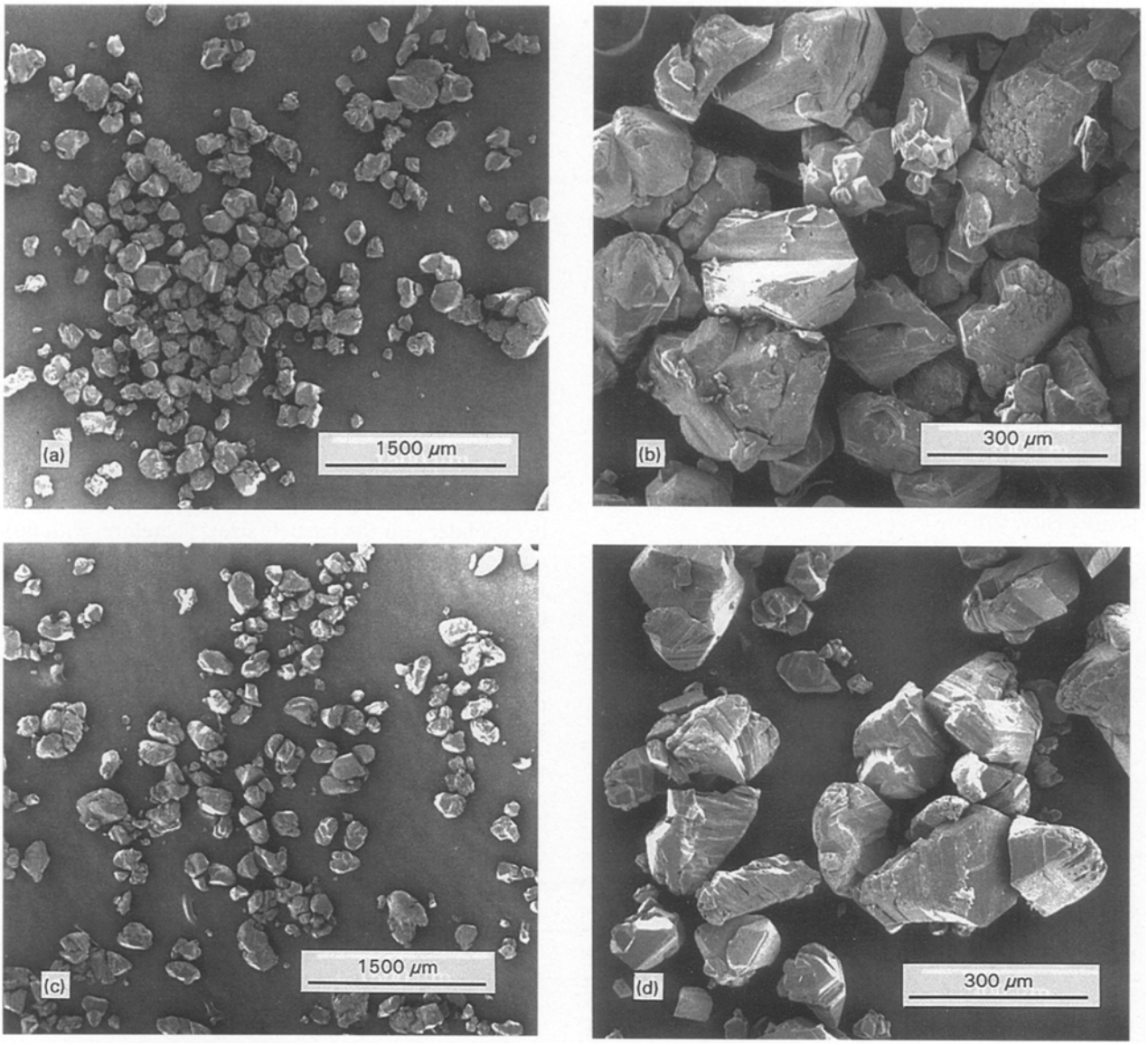

Figure 5 SEM's at two magnifications (17× and 87×) of TATB crystals grown from stirred saturated solutions with (a) and (b) a constant dS/dt cooldown rate, and (c) and (d) an accelerated dS/dt cooldown rate.

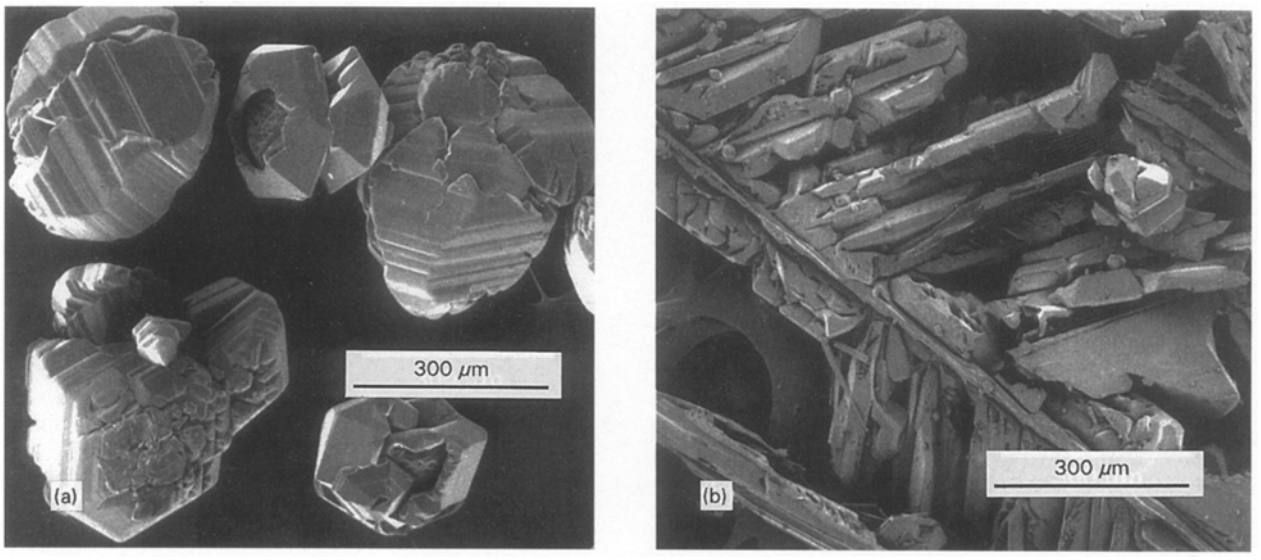

Figure 6 SEM's (87×) of TATB crystals grown from saturated solution that was (a) stirred vigorously and (b) not stirred during cooldown.

in bulk solution, at edge of boundary layer, mol m^{-3}, C_s = TATB concentration in solution at particle surface, mol m^{-3}.

For TATB crystallizing on a spherical particle, the rate of change of the particle radius is given by the volumetric flux to the surface (calculated from the molar flux, molecular weight, and density of TATB) divided by the surface area of the particle:

$$\frac{dr_1}{dt} = \frac{CDM_w}{\rho} \times \ln\left(\frac{C_\infty}{C_s}\right) \times \left(\frac{r_2}{r_1}\right) \times \left(\frac{1}{r_2 - r_1}\right) \quad (2)$$

where, in addition to the definitions above: (dr_1/dt) = rate of change of particle radius, m s^{-1}, t = time, s, M_w = molecular weight of TATB, g mol^{-1}, ρ = density, g m^{-3}.

To relate Equation (2) to stirring speed, a slow stirring speed will give a thick stagnant boundary layer around the particle, and $r_2 \gg r_1$. In this case,

$$\frac{dr_1}{dt} = \frac{CDM_w}{\rho} \times \ln\left(\frac{C_\infty}{C_s}\right) \times \frac{1}{r_1} \quad \text{for slow stirring.} \quad (3)$$

With fast stirring, the stagnant boundary layer is thin, $r_2 \approx r_1$, and

$$\frac{dr_1}{dt} = \frac{CDM_w}{\rho} \times \ln\left(\frac{C_\infty}{C_s}\right) \times \frac{1}{(r_2 - r_1)}$$

for fast stirring. (4)

From Equation (3), the rate of absolute radial particle growth with slow stirring is faster for smaller particles than for larger particles. After the initial particles nucleate from the cooling solution, the smaller particles will preferentially remove the dissolved TATB from solution, larger particles will grow very slowly, and the resultant particle size distribution will have a large number of small particles and few large particles. By contrast, with fast stirring, the growth rate is essentially independent of particle size (the thickness of the stagnant boundary layer is only slightly dependent on the particle size). Therefore, with fast stirring, all particles will grow at the same absolute radial rate, allowing more large particles to form in comparison to slow stirring.

The above analysis is consistent with our results as shown in Table I and Fig. 4. From the data with constant dS/dt, runs with slow or medium stirring rate showed a large fraction (9–25%) of particles < 200 μm, while runs with fast stirring showed a small

TABLE II Particle-size data for size regeneration study

Material	Ultrafine	2×	1.5×	Normal	1×
Particle size (mm)	Weight fraction				
0.1180–0.1020	0.0000	0.0000	0.0000	0.0114	0.0696
0.1020–0.0881	0.0000	0.0000	0.0000	0.0314	0.1710
0.0881–0.0760	0.0000	0.0000	0.0000	0.0477	0.2210
0.0760–0.0656	0.0000	0.0000	0.0073	0.0599	0.2160
0.0656–0.0566	0.0001	0.0013	0.0279	0.0687	0.1590
0.0566–0.0488	0.0008	0.0132	0.0556	0.0846	0.0662
0.0488–0.0421	0.0011	0.0180	0.0740	0.0995	0.0257
0.0421–0.0363	0.0013	0.0195	0.0755	0.0987	0.0249
0.0363–0.0313	0.0049	0.0454	0.0966	0.0728	0.0172
0.0313–0.0270	0.0086	0.0716	0.1180	0.0465	0.0094
0.0270–0.0233	0.0116	0.0785	0.1110	0.0429	0.0077
0.0233–0.0201	0.0192	0.0943	0.0903	0.0374	0.0045
0.0201–0.0174	0.0230	0.0913	0.0768	0.0353	0.0034
0.0174–0.0150	0.0312	0.0840	0.0585	0.0357	0.0025
0.0150–0.0129	0.0388	0.0858	0.0516	0.0340	0.0015
0.0129–0.0111	0.0478	0.0881	0.0445	0.0305	0.0001
0.0111–0.00962	0.0542	0.0742	0.0310	0.0262	0.0000
0.00962–0.00830	0.0634	0.0648	0.0227	0.0248	0.0000
0.00830–0.00716	0.0719	0.0438	0.0154	0.0228	0.0000
0.00716–0.00618	0.0748	0.0344	0.0123	0.0206	0.0000
0.00618–0.00533	0.0759	0.0300	0.0110	0.0176	0.0000
0.00533–0.00460	0.0781	0.0246	0.0087	0.0142	0.0000
0.00460–0.00397	0.0692	0.0188	0.0064	0.0109	0.0000
0.00397–0.00342	0.0607	0.0101	0.0034	0.0080	0.0000
0.00342–0.00295	0.0554	0.0051	0.0015	0.0060	0.0000
0.00295–0.00255	0.0535	0.0022	0.0002	0.0043	0.0000
0.00255–0.00220	0.0702	0.0008	0.0000	0.0039	0.0000
0.00220–0.00190	0.0690	0.0000	0.0000	0.0031	0.0000
0.00190–0.00164	0.0182	0.0000	0.0000	0.0007	0.0000
0.00164–0.00141	0.0022	0.0000	0.0000	0.0000	0.0000
0.00141–0.00122	0.0001	0.0000	0.0000	0.0000	0.0000
< 0.00122	0.0000	0.0000	0.0000	0.0000	0.0000
Fig. 7:	a	b	c	d	e

fraction (3–7%) of particles <200 μm. Similarly, runs with slow or medium stirring rate showed fewer large particles (9–15% >300 μm) than runs with fast stirring (12–29% >300 μm). In general, the runs with fast stirring showed a broader distribution of particle sizes, since particles of all initial sizes grew uniformly. Based on the preceding theoretical and experimental evidence, we therefore generalize that faster stirring is desirable for production of large particles or a broad particle size distribution, while slow stirring is better for formation of small particles.

Seed crystals of 200–500 μm particle size were added in two runs. The intent was to provide nucleation sites for deposition of dissolved TATB as the solution cooled, thereby preventing nucleation of new crystals and leading to formation of fewer large crystals. To select the mass of seed crystals to add, we used 500 μm as a target crystal size, and calculated that the entire 23 g of material would give about 190 000 particles of this diameter. To add this number of seed crystals would require 2.3 g of 200–250 μm TATB crystals. We added less (~ 1.1 g) crystals in the 200–246 μm range than required to the run labelled 4e, because of our limited supply of crystals in this size range. In this run, the number of 200–246 μm particles was increased, but the number of smaller particles was not reduced and the number of particles over 300 μm was decreased. Similarly, we added ~ 2 g of crystals in the 300–500 μm range to the run labelled 4 g, and saw a comparable effect. We also see this when we compare data in Table I for runs 4(e, g), with seeds, to 4(f, h, i) without. Therefore, the addition of seed crystals was not effective in producing larger crystals, but did lead to a narrower particle size distribution.

In this work reducing the number of heating mantles from two to one did not affect crystal growth, but did allow better control over temperature overshoot. In our earlier crystallization study [8] we found that a few weight percent BHT added to the DMSO solution acted as a radical scavenger and/or inhibitor, as well as a morphology modifier. In this study, we saw no significant change in crystal size or shape for the BHT concentrations of 1.5×10^{-2}–3.7×10^{-3} M (TATB:BHT molar ratios of 4:1–1:1 respectively).

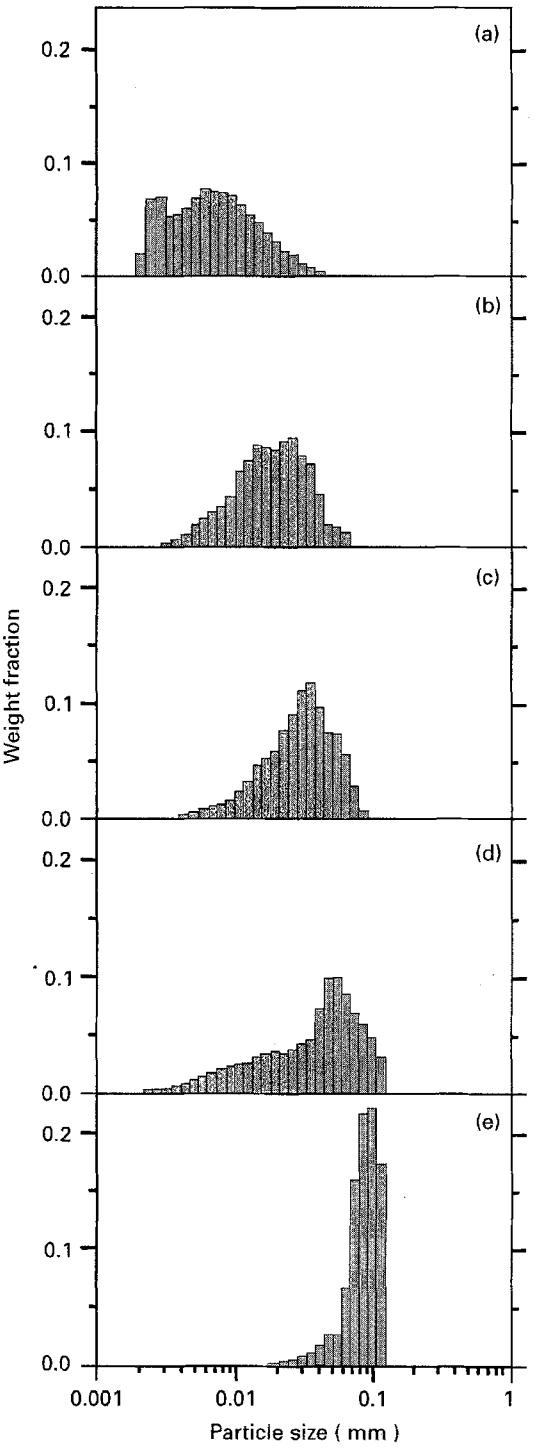

Figure 7 Particle-size distributions determined by the Malvern particle-size analyzer of samples of (a) starting ultrafine TATB, and of TATB grown with vigorous stirring from (b) 2× saturated, (c) 1.5× saturated, (d) "normal" target crystal size TATB, and (e) just saturated solutions.

3.2. Size regeneration

The crystal size distribution data obtained with the Malvern particle-size analyzer are shown in Table II as a function of saturation, and are also shown in Fig. 7 (b, c, e). The particle size distribution for one batch that was not stirred is not shown. Also given for comparison (Table II, Fig. 7(a, d)) are distributions of the ultrafine starting material and a typical batch of "normal" target crystal size TATB (water-aminated [2] LLNL internal batch number C-084). The most notable shift seen in the particle-size distribution, however, resulted from changing the degree of solution saturation. Fig. 8(a–d) show same magnification SEM's of the ultrafine starting material and crystals grown from solutions that are 2×, 1.5×, and just saturated by weight. Their corresponding distributions are shown to successfully bracket the target particle sizes of ~ 50–70 μm. By adjusting the degree of supersaturation to something less than 1.5×, it would be possible to achieve particle-size regeneration. Runs with supersaturation are effectively being seeded with many very small seed crystals. Like the results described earlier with large seed crystals, the use of many small seeds did not lead to formation of large particles. The effect of stirring during cooldown was again found to be important in affecting crystal morphology. Crystals grown with fast stirring appeared as pyramid to irregular shaped chunks, while

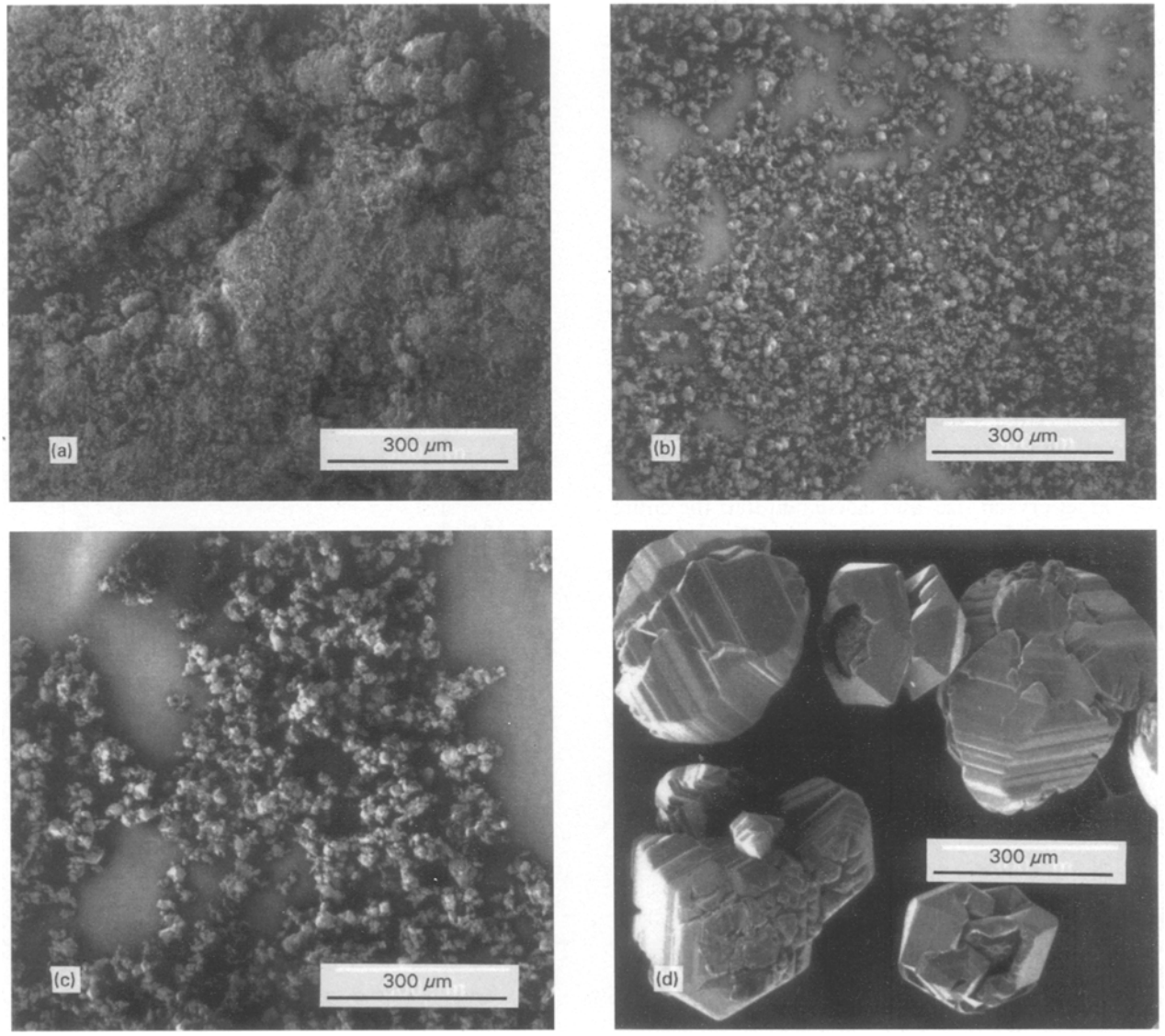

Figure 8 87× magnification SEM's of (a) starting ultrafine TATB and of TATB crystals grown (b) from 2× saturated solution, (c) from 1.5× saturated solution, and (d) from saturated solution.

those grown with no stirring during cooldown were needle-like (Fig. 6). The needle-like crystals are unacceptable for PEX formulations because of undesirable flow properties.

There appears to be a dichotomy in crystal morphology between those crystals grown under supersaturation conditions and those from the solution taken just to saturation. In Fig. 9b and c the crystal surfaces grown under supersaturation appear smooth and relatively defect-free. In Fig. 8c, the crystals grown from saturation have surfaces that are irregular and the shapes non-uniform. Therefore it appears that the degree of saturation had an effect on crystal morphology. We note, however, that the saturated solution crystals were run from solvent, reused from the previous study, which had not been cleaned with activated charcoal. In that study, it was noted that the reuse of uncleaned DMSO produced successive batches of crystals discoloured slightly to orange. With activated charcoal treatment of the solution between later runs with supersaturation in this study, however, neither the solution nor later crystals became discoloured. The better quality crystals from supersaturated solutions produced in this study may have resulted from the lower concentration of dissolved impurities in the solvent (i.e. fewer impurity-induced defects in the crystal lattice).

4. Summary

Up to 46 g batches of the insensitive explosive TATB have been recrystallized from DMSO in an effort to prepare larger particle-size material. The first part of the study investigated conditions required to shift the particle-size distribution maximum from ~50–70 μm to several hundred micrometres in diameter. Distributions peaking at ~200–246 μm were successfully produced by varying the cooldown rate and degree of agitation during cooling. Solution agitation during the cooldown cycle was found to be important to get crystals that better approximated the ideal spherical shape, as well as to attain the larger particle size distributions. Based on mass transfer considerations, we can generalize that faster stirring produces large particles or a broad particle size distribution, while slow stirring tends to form small particles. The rate of cooling, and

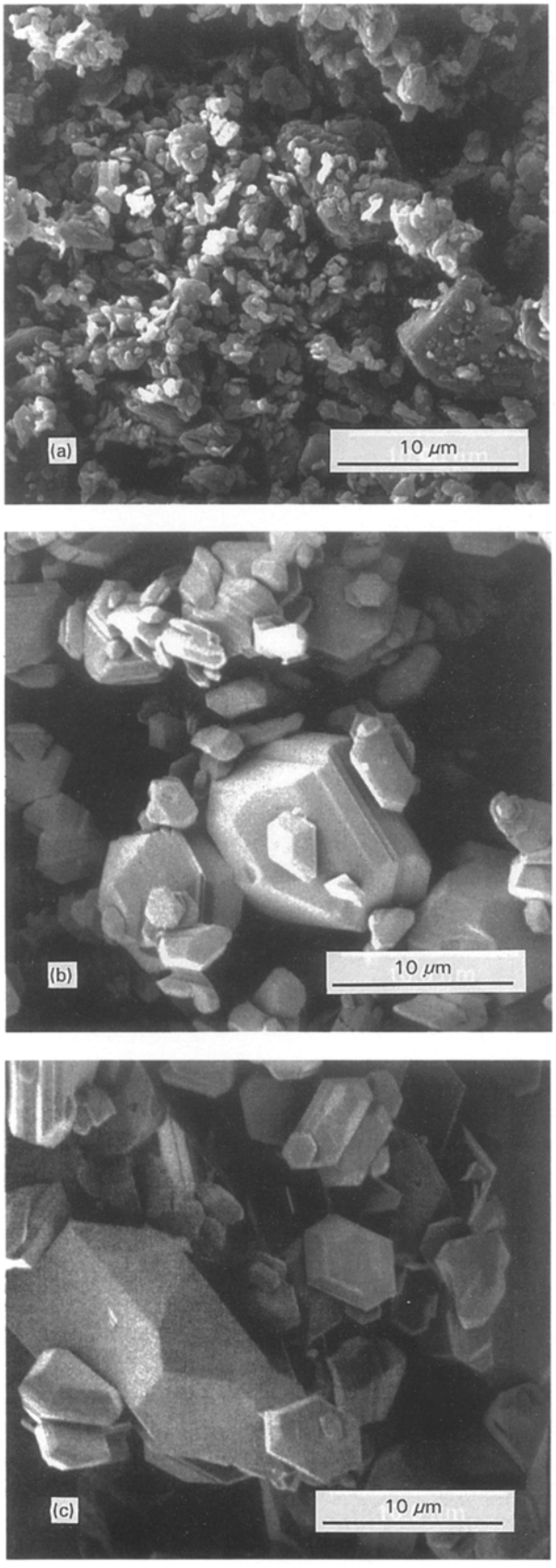

Figure 9 Higher magnification (2600×) SEM's of TATB particles from (a) the starting ultrafine TATB material, (b) from 2× saturated solution, and (c) from 1.5× saturated solution showing regular well-formed surfaces.

therefore the rate of change in solubility (dS/dt), was also found to affect the sharpness of the particle-size distribution. The narrowest distribution (Fig. 4f) was produced when cooling followed an accelerated dS/dt curve.

The second part of the study emphasized regeneration of the standard ~50–70 μm distribution from ultrafine TATB. By changing the degree of solution saturation from just saturated to 2× saturated, distributions were grown that successfully bracketed the desired particle-size distribution. By cleaning the solvent between runs with activated charcoal to remove thermal degradation products, the colour of the product TATB crystals remained constant and good crystal morphology was maintained with consecutive batches.

There were a number of questions not addressed in this study that should be resolved if further scale-up is attempted. The chemical purity of crystals made by this method should be determined (i.e. total chlorine and chlorinated nitroaromatics, and total sulfur content) and compared against specifications [2]. The small-scale safety test values and shock sensitivity of crystallized TATB should be compared with those of "normal" TATB. Formulation properties are also unknown: if the crystal surfaces are very smooth or chemically modified, will the binder be able to bond well? The effect of contamination by green TATB is unknown. It was found in the earlier study that the presence of TATB turned green from UV-irradiation yielded an orange-discoloured product; it was concluded that the presence or formation of radicals, important in this thermal degradation, is retarded by the preventative addition of small amounts of the radical scavenger BHT and removal of metallic surfaces [8]. The extent to which contamination can be tolerated without lowering chemical purity or degrading crystal quality, or how to most efficiently purify "green TATB" prior to processing, was not determined in either study.

Acknowledgements

The authors wish to gratefully acknowledge César Pruneda and Mark Hoffman for their invaluable insights on TATB and formulations, Jim Yoshiyama for the scanning electron micrographs, Ted Jessop for the Malvern particle-size analysis, and the Nuclear Safety Program for funding. This work was performed under the auspices of the U.S. Dept. of Energy by Lawrence Livermore National Laboratory under contract No. W-7405-ENG-48.

References

1. B. M. DOBRATZ, "LLNL Explosives Handbook: Properties of Chemical Explosives and Explosive Simulants", UCRL-52997 Change 2, Lawrence Livermore National Laboratory, Livermore, CA, Jan. 1990.
2. "Material Specifications for TATB", Drawing No. 13Y-188025 (Revision 2) Los Alamos National Laboratory, Los Alamos, NM, June 1983.
3. "Specification for Ultrafine TATB", Drawing No. RM254959 (Issue B), Los Alamos National Laboratory, Los Alamos, NM, Dec. 1981.
4. A. E. OBERTH, "Principles of Solid Propellant Development", CPIA Publication 469, The Johns Hopkins University, Laurel, MD, Sept. 1987, Chapter 5.
5. D. M. HOFFMAN, L. SPELLMAN, C. M. WALKUP and W. C. TAO, "Next Generation Insensitive, "Tough" Extrusion

Cast Explosive (ITECX)", Lawrence Livermore National Laboratory, Livermore, CA, in preparation.
6. W. SELIG, "How to Estimate the Solubility of an Insoluble Compound – 1,3,5-Triamino-2,4,6-Trinitrobenzene (TATB)", UCID-17412, Rev. 1, Lawrence Livermore National Laboratory, Livemore, CA, Apr. 1977.
7. T. M. BENZIGER and R. K. ROHWER, "Pilot Plant Production of Triaminotrinitrobenzene (TATB)", LA-3632, Los Alamos Scientific Laboratory, Los Alamos, NM, Nov. 1966.
8. M. F. FOLTZ, D. L. ORNELLAS and P. F. PAGORIA, "Small-scale Recrystallization and Solubility of 1,3,5-Triamino-2,4,6-trinitrobenzene in DMSO", UCRL-JC-116398, Lawrence Livermore National Laboratory, Livermore, CA, Feb. 1994.
9. K. J. SCRIBNER, "HMX Particle Size Analysis, Round Robin", UCRL-ID-110679, Lawrence Livermore National Laboratory, Livermore, CA, June 1992.
10. D. M. HOFFMAN, Lawrence Livermore National Laboratory, personal communication, 1993.
11. R. B. BYRD, W. E. STEWART and E. N. LIGHTFOOT, Transport Phenomena (Wiley & Sons, New York, 1960) p. 528.

Received 12 October 1994
and accepted 8 September 1995